JOURNAL OF AIRCRAFT
Vol. 47, No. 4, July–August 2010

FENSAP-ICE: Analytical Model for Spatial and Temporal Evolution of In-Flight Icing Roughness

Giulio Croce* and Erika De Candido†
Università di Udine, 33100 Udine, Italy
Wagdi G. Habashi‡ and Jeffrey Munzar§
McGill University, Montreal, Quebec H3A 2S6, Canada
and
Martin S. Aubé,¶ Guido S. Baruzzi,** and Cristhian Aliaga††
Newmerical Technologies International, Montreal, Quebec H3A 2M7, Canada

DOI: 10.2514/1.47143

Ice roughness, which has a major influence on in-flight icing heat transfer and, hence, ice shapes, is generally input from empirical correlations to numerical simulations. It is given as uniform in space, while sometimes being varied in time. In this paper, a predictive model for roughness evolution in both space and time during in-flight icing is presented. The distribution is determined mathematically via a Lagrangian model that accounts for the stochastic process of bead nucleation, growth, and coalescence into moving droplets and/or rivulets and/or water film. This general model matches well the spatial and temporal roughness distributions observed in icing tunnel experiments and is embedded in FENSAP-ICE, extending its applicability outside the range of airfoil types for which correlations exist. Thus, an additional important step has been taken toward removing another empirical aspect of in-flight icing simulation.

Nomenclature

g	=	gravity
h	=	height
L	=	latent heat
m	=	mass flow
p	=	pressure
Q_h	=	convective heat flux
T	=	temperature
u, v	=	velocity
β	=	collection efficiency
μ	=	viscosity
ρ	=	density of water
τ	=	shear stress

I. Introduction

IN-FLIGHT icing continues to represent major risks for aircraft safety. When an airplane crosses clouds of supercooled droplets during takeoff, holding, or landing, the impinging droplets may freeze on the exposed surfaces and build up ice around wings, nacelles, tail, empennage, antennas, and several other lifting and nonlifting areas. The accreted ice may alter the aerodynamic performance of the aircraft, interfere with the movement of control surfaces and their effectiveness, block engine inlets, or be shed and damage engines, propellers, or structural components.

Computational fluid dynamics (CFD) modeling has emerged as a powerful tool for the prediction of ice shapes and for the simulation and optimization of ice protection systems. However, the simulation of in-flight icing is a very complex multiphysics problem, and several aspects are still far from being well represented. The present paper borrows ideas in a multidisciplinary way from various fields to elucidate one of these issues, namely, the analytical versus empirical evaluation of ice-induced surface roughness, which has an important effect on conjugate heat transfer and, ultimately, on accreted ice shapes. FENSAP-ICE, a 3-D in-flight icing system, serves as the ideal vehicle for the new models developed.

Experimental evidence shows that an iced surface is not smooth, but covered by a collection of nearly hemispherical beads with radii of the order of millimeters [1]. Furthermore, because roughness is induced by the ice accretion itself, it is far from being constant in either space or time. In particular, roughness appears at the beginning of ice formation and grows with time until a final distribution is attained asymptotically [2]. Roughness height is also not constant in space but is usually very small around the leading edge and becomes larger further downstream [1,3].

The roughness shape and distribution ought to be intuitively related to the size and evolution of the beads and rivulets formed on the surface by impinging droplets and their interaction with the already accreted layer. Surface roughness affects shear stress and heat transfer [4], which in turn determine the shape and size of the accreted ice layer. Thus, there is a time-varying two-way coupling between roughness buildup and ice accretion. Finally, the liquid water layer on the ice surface affects the effective area exposed to evaporation and, consequently, the evaporative heat flux. The importance of the effective surface fraction exposed to evaporation in heat transfer processes has been clearly demonstrated in different application fields [5,6] and should not be neglected in the simulation of anti- and de-icing systems.

The understanding and handling of ice-induced roughness is of crucial importance to obtain accurate and reliable CFD-based ice shapes. Currently, most icing codes provide simplified roughness modeling through the use of empirical correlations. The most widely employed correlation is that of Shin and Bond [7], which gives a

Presented as Paper 2009-4126 at the 1st AIAA Atmospheric and Space Environments Conference, San Antonio, TX, 22–25 June 2009; received 11 September 2009; revision received 31 December 2009; accepted for publication 12 January 2010.

*Professor, Department of Mechanical Engineering, Via delle Scienze 208.
†Ph.D. Candidate, Department of Mechanical Engineering, Via delle Scienze 208.
‡Professor, Director of the Computational Fluid Dynamics Laboratory, Department of Mechanical Engineering, 688 Sherbrooke Street West, Fellow AIAA.
§Honors Summer Student, Computational Fluid Dynamics Laboratory, Department of Mechanical Engineering, 688 Sherbrooke Street West.
¶Vice President Operations, 680 Sherbrooke Street West.
**Director of Product Development, 680 Sherbrooke Street West. Member AIAA.
††Chief, Consulting Services, 680 Sherbrooke Street West.

single, average, representative value of roughness as a function of cloud liquid water content (LWC), droplet mean volumetric diameter (MVD), temperature, and aircraft speed. This very useful correlation was deduced empirically from the analysis of a very large number of experimental ice shapes, but is validated only for airfoils with chord lengths greater than 14 in. By their own nature, these empirical correlations must reduce the complexity of the physical phenomenon by delivering a single constant value; they are unable to take advantage of the wealth of local flow details available from CFD computations and are limited to the geometries for which the ice accretion characteristics have been measured. They are of limited range and cannot be generalized to propellers, rotors, helicopters, nacelles, and turbomachinery blades, which are all components that are of immense interest to the icing community.

Therefore, for a more general ice roughness model to emerge, a detailed simulation of the physics of water and ice is needed. Although this detailed simulation might be seen to increase the computational effort and time, this pales when compared to the prohibitive cost of conducting experiments to obtain proper roughness correlations for the most general cases.

Such detailed simulation must be derived from a microphysical modeling of the evolution of the water layer, taking into account surface tension effects, transition among stationary beads, flowing rivulets, and continuous water film. In essence, the microphysical behavior of water is controlled primarily by the interaction of surface tension forces with aerodynamic and gravity forces. Surface tension tends to inhibit bead movement and to minimize the area wetted by the fluid, forcing water to coalesce into larger beads or into rivulets. Shear stress, pressure gradients, and gravitational forces, on the other hand, trigger bead motion. For high incoming droplet flow rates on wettable surfaces, the water will completely coat the entire solid surface, whereas in the opposite case, surface tension will cause the water to form beads, whose freezing will consequently yield an ice-induced roughness.

A promising attempt was recently proposed by Fortin et al. [8], who proposed an analytical model for the computation of surface roughness, runback, and shedding water on an airfoil surface. Their physical model is based on the work of Hansman and Turnock [9], who defined roughness elements as beads and measured contact angles of water on ice. The beading model proposed in [8] provides bead growth and evolution with time, but the water-layer description remains simplified: water in the impingement areas of the airfoil can only exist in the form of stationary beads or a flowing film, whereas outside the impingement areas, rivulets or continuous film are allowed, assuming the maximum bead height as the threshold value to discriminate between the two regimes. Furthermore, this roughness model seems not to have been validated against experimental data.

The present paper extends this promising approach into a more comprehensive description of ice roughness. The beading model in Fortin et al. [8] is taken as a starting point and enhanced with a slightly different description of the possible transitions from water beads to rivulets to continuous film. New criteria, derived from a balance of the applied forces, have been introduced to account for the local state of the water. Furthermore, an analysis of the statistical distribution of bead sizes is first done with a Lagrangian-style model. The results offer a description of the average behavior of the beads, which has been incorporated into the FENSAP-ICE system. The roughness height values predicted by the model have been compared to experimental data and the results are quite reproducible over the range of data.

II. Ice Accretion Model

The present modeling effort is fully integrated into the FENSAP-ICE system [10]. In FENSAP-ICE, both the external flowfield and the droplet flow are computed via an Eulerian approach and a finite element discretization on a 3-D computational grid. Once the impingement areas have been determined, a heat and mass balance module (ICE3D), derived from the Messinger model [11], determines the amount of water that will freeze, run back or evaporate, as well as its temperature. The water-layer computation is performed via a control-volume discretization on the 2-D curved surface at the air/solid interface, as shown in Fig. 1. The original 3-D mesh around the object is then modified to locally account for the mass of ice accreted, and finally the flow around the modified object is computed again. Iterating between these steps will produce a realistic prediction of the ice shape growth history.

The mathematical expression for the energy balance in ICE3D states that

$$\rho\left[\frac{\partial h_f c_w \bar{T}}{\partial t} + \mathrm{div}(\bar{u}_f h_f c_w \bar{T})\right] = \left[c_w \bar{T}_d + \frac{(\|v_d\|)^2}{2}\right] \times U_\infty LWC\beta - 0.5(L_{\mathrm{evap}} + L_{\mathrm{subl}})\dot{m}_{\mathrm{evap}} + (L_{\mathrm{fusion}} - C_{\mathrm{ice}}\bar{T})\dot{m}_{\mathrm{ice}} + \sigma(T_\infty^4 - T^4) + \dot{Q}_h \quad (1)$$

where the first three terms on the right-hand side model the heat transfer generated by impinging supercooled water droplets, by evaporation, and by ice accretion. The last two terms are the radiative and convective heat transfer. The subscripts f and d refer, respectively, to the water film and incoming droplets.

The convective terms in Eq. (1) are obviously strongly dependent on the behavior of the surface water layer, because water impinges on the exposed surfaces as a collection of supercooled droplets carried by the airflow. On impact with a solid surface, the droplets could deposit as stationary beads, flow along the surface as individual beads, coalesce into larger beads, or flow as rivulets. For a sufficiently large impinging water mass flow, a continuous liquid water film may appear.

The different regimes are defined by the equilibrium between surface tension, which opposes water flow and promotes coalescence, and external forces (mainly shear stress, with locally relevant contributions from gravity and pressure gradients) that promote droplet movement. Because the external forces are proportional to either the cube or the square of the radius, R^3 or R^2, and the surface tension to the radius R, bead movement will only occur above a threshold value of R.

In the case of stationary beads there is no mass transport at all, and the corresponding terms in Eq. (1) will vanish. Furthermore, because the beads have a statistical size distribution, not all of them will reach the threshold radius for movement at the same time. Thus, at the beginning of the process, only a fraction of the incoming mass will flow along the surface:

$$\mathrm{div}\,(\bar{u}_f h_f) = \mathrm{div}\left[\bar{u}_f h_f \frac{\mathrm{WM}_{\mathrm{moving}}}{\mathrm{WM}_{\mathrm{still}}}\right] \quad (2)$$

where WM is the water mass.

Furthermore, the details of the beads/rivulet geometry have an impact on heat transfer, because they affect the effective area for heat and mass transfer. In Eq. (1), the terms of the evaporative and freezing mass flow, as well as the convective heat transfer contribution, should be altered to account for the bead surfaces, as indicated in Fig. 2.

For example, if the evaporative mass flow is computed using the heat and mass transfer analogy, the corresponding term should be

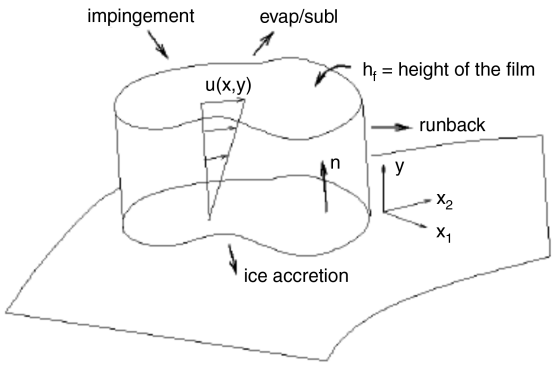

Fig. 1 Characteristics of the water-layer model.

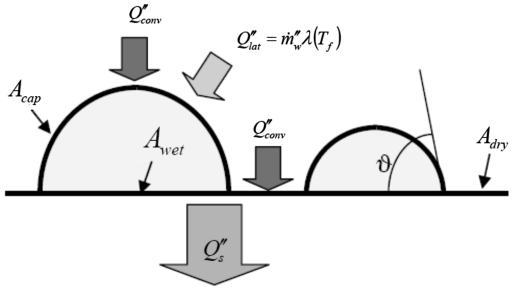

Fig. 2 Drops, heat fluxes, and exchange areas.

corrected by the ratio between the actual surface exposed to evaporation and the clean object surface.

Finally, if freezing takes place in the presence of stationary or moving beads, the surface roughness will be closely related to the size of the beads themselves. Roughness, on the other hand, will affect the convective heat transfer and wall shear stress, inducing a two-way coupling between bead formation and airflow. This coupling is even more evident during the ice accretion process, when the ice shape itself is heavily influenced by the roughness. As an example, within FENSAP-ICE, turbulence is usually successfully described via the Spalart–Allmaras model. Following such an approach, roughness effects are taken into account via a correction based on a length scale related to the aforementioned equivalent sand-grain height. Even assuming a constant value in space and time, the proper choice of this value has a significant impact on the ice shape prediction, as demonstrated in [10]. The use of a more realistic value, that varies in both space and time, is thus expected to offer a significant departure from empiricism.

The mass conservation equation for the water layer is expressed as

$$\rho\left[\frac{\partial h_f}{\partial t} + \mathrm{div}(\bar{u}_f h_f)\right] = U_\infty \mathrm{LWC}\beta - \dot{m}_{\mathrm{evap}} - \dot{m}_{\mathrm{ice}} \qquad (3)$$

where the three terms on the right-hand side correspond, respectively, to the mass transfer due to droplet impingement, evaporation, and ice deposition. The terms affected by roughness are the same as for the energy equation. Compatibility relations are needed to close the system, as described in [10].

III. Beading Model for Glaze Icing Conditions

When a supercooled droplet impacts on a solid surface at glaze icing subfreezing temperatures, only a part of it will freeze, and even then, not instantaneously: a water bead forms and grows through the contribution of the impinging droplets and by coalescence with other beads. The growth of the bead, which could also be partially frozen, stops when the aerodynamic and gravitational forces overwhelm the water surface tension. At that time, the bead flows away as a running droplet or coalesces into a rivulet or a continuous film. To mimic the bead growth and coalescence processes, which determine the time evolution of surface roughness, it is useful to consider the analogy between coalescence of water beads on an aircraft surface and the coalescence of the tiny droplets that originate during condensation processes. The latter has been described in detail by Beysens [12].

From experimental evidence it is recognized that coalescence during condensation (air moisture on a low-temperature solid surface) is a self-similar process in the sense that the average characteristics of a droplet pattern at different times are identical (statistically speaking) and exhibit universal features. When surface coverage (ratio of wet to total areas) exceeds 30%, coalescence of neighboring beads takes place and frees area to allow new nucleation, leading to an increase in the growth of the median diameter. As coalescence continues, the surface coverage increases asymptotically until it reaches a universal value of 55%.

Returning to in-flight beading, we assume that the coalescence process is similar to that observed during condensation: droplet impingement at random locations is equivalent to nucleation, and just as drops in condensation grow by coalescence and direct condensation on their surfaces, beads on an aircraft surface will grow through the contribution of new droplet impacts and coalescence with neighboring ones. When surface coverage exceeds a certain value, the probability of impinging droplets merging with existing beads increases and the growing beads will begin to coalesce with their neighbors and release dry areas for new impinging drops.

This coalescence/growth model was tested for a simple configuration, namely, droplets impinging at random locations on a vertical surface. Each individual bead is tracked by a Lagrangian approach during its growth, until movement begins. The impinging droplet flow rate is defined by drop diameter, LWC, and air speed. Coalescence occurs if a new droplet lands on an existing bead or if the perimeters of two existing beads overlap one another. Coalescence will generate a new bead with the center of mass and total volume of the two original beads. When the bead size is large enough, the gravity force exceeds the surface tension and the bead is swept away, freeing a dry area for new impinging droplets.

The simulation shows that surface coverage grows with respect to time until it reaches a maximum value between 80 and 90% in all the cases tested, irrespective of input parameters (drop diameter, LWC, and airspeed). When surface coverage becomes constant, the incoming mass flow induces a growth in the average bead, which triggers its movement. A steady-state condition is attained when new impinging droplets constantly replace beads leaving the computational domain. In the absence of freezing water, steady-state surface coverage is significantly lower than the maximum value and approaches the limit observed by Beysens [12] for condensation (around 55%). Under icing conditions, this reduction is much smaller, if not totally absent, because a large number of beads freeze before movement, as shown in Fig. 3. We assume here that an impinging droplet at first generates a bead, which will grow and coalesce with other beads and partially freeze.

This Lagrangian separate computation is preliminarily run off-line to provide useful information to formulate a model of the process within the fully Eulerian framework of ICE3D. It is important to clarify that it does not have to be repeated for every single analysis. In particular, the average bead radius initially increases linearly with time, until the maximum surface coverage (85%) is reached. Later on, the same radius is computed from the total mass present on each computational element, Eq. (2), and the assumption of fixed surface coverage.

A. Bead Maximum Size

The definition of the thresholds for bead movement, film onset, and rivulet formation requires a balance of the forces acting on the bead.

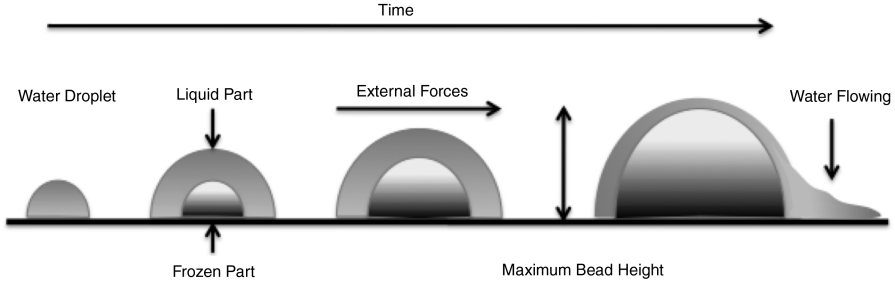

Fig. 3 Droplet evolution.

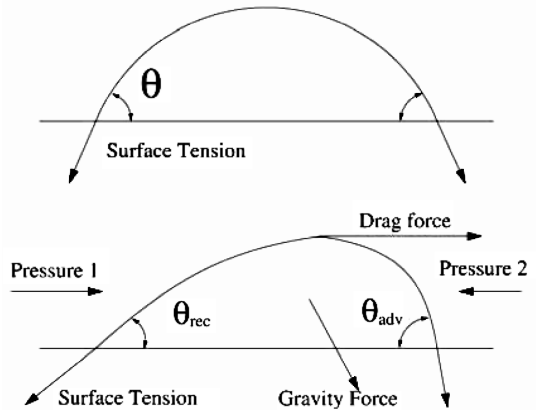

Fig. 4 Deformed and undeformed bead, forces and relevant angles.

The external forces acting on a bead are the shear stress exerted by the airflow (F_d), the gravitational force (F_g), and the pressure gradient along the profile (F_p), which is quite negligible everywhere except at the leading edge. The bead's surface tension (F_σ) will resist movement. Hence,

$$\sqrt{\sum_{i=1}^{3}(F_{d_{xi}} + F_{g_{xi}} + F_{p_{xi}})^2} = F_\sigma \tag{4}$$

The bead deforms under the effect of the forces, changing to a nonspherical shape, as illustrated in Fig. 4 (see also Fortin et al. [8] for comparison). The advancing and receding contact angles describe the deformed bead geometry, with the bead rigidity being proportional to the difference between these two angles. The surface tension is oriented against the resultant of the external forces acting on the bead; this direction is referred to as the movement axis.

The force is found by integrating the projection of the surface tension on the movement axis along the contact line:

$$F_\sigma = \int_0^\pi \sigma \cos(\theta(\varphi)) \cos(\varphi) r \, \mathrm{d}\varphi \tag{5}$$

It is necessary to have an expression for the variation of the contact angle along the contact line. According to the experimental observations of El Sherbini and Jacobi [13], the contact angle $\vartheta(\varphi)$ is a third-degree polynomial that is a function of the advancing and receding contact angles ϑ_{adv} and ϑ_{rec}. It must be underlined that bead rigidity is expressed here in terms of physical constants and bead height. All the other forces are also function of the bead height, which can therefore be taken as the threshold value for bead movement.

The components of the gravitational force as a function of the bead height are defined as

$$F_{g_i} = \pi\left(\frac{1}{1-\cos(\vartheta)} - \frac{1}{3}\right)\rho g_i h_{\text{bead}}^3 \tag{6}$$

Also, the force exerted by the airflow on the bead and the pressure gradient force can be expressed as a function of contact angle.

By equating the external forces acting on the bead, it is possible to solve for the maximum bead height. The body-force balance described earlier also holds true when considering partially frozen beads. The freezing process starts from the bottom/center of the bead, so that the outer part of the bead will be liquid, and all the forces acting on the bead are surface forces, with the exception of gravity, which will be taken into account only for the liquid part of the bead.

The ice roughness is related to the computed bead size; the bead height will be considered as the roughness height for all the different stages of bead growth, until it reaches the maximum size. When water begins to flow, the height of the frozen part of the bead will be considered to be the roughness height, provided that it does not exceed the maximum allowed bead height. This assumption is made according to experimental evidence: during the ice accretion process, the roughness reaches a maximum height and then remains constant with time. The hypothesis is that, as time elapses, the dynamics of the beads on the frozen surface is self-similar. Beads will coalesce and freeze near other frozen beads, filling the gaps and growing, layer by layer, in a similar way. Finally, the modifications to the continuity and energy equations, described in Sec. II, are introduced: the evaporation term is modified by introducing the ratio of the effective exposed area to the solid area, as in [5,6].

As stated earlier, due to the statistical distribution of bead sizes, beads will not begin moving in unison: larger beads begin to move before the average radius reaches the threshold, whereas smaller ones will not move until the average radius gets significantly larger than the threshold. The distribution obtained form the aforementioned Lagrangian model indicates that incipient motion appears at an average radius equal to 65% of the threshold. This is consistent with the observation of Olsen and Walker [14], who detected the onset of runback throughout a similar range of average bead diameters; however, they ascribed this to unpredictable imperfections of the solid surface, which have a direct influence on surface tension and contact angles and, therefore, induce random variations in the maximum threshold bead size given by Eq. (4) for each individual bead. In any case, we assume that movement is a gradual process: once the maximum bead height in a cell exceeds the movement threshold, the runback water fraction is assumed proportional to the ratio between instantaneous average and maximum bead height.

B. Moving Beads, Rivulets, and Film

When the external forces overcome the surface tension and the bead starts to move, we can expect intuitively that it will flow as a rivulet or a continuous film, depending on the water content of the surface, that is, moving beads will coalesce into rivulets, which in

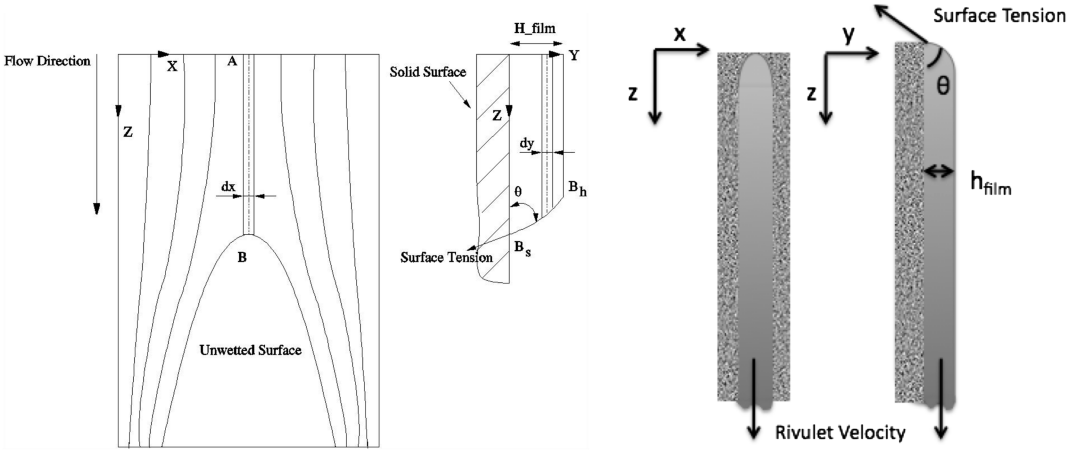

Fig. 5 Film flowing on a vertical plate, according to [15]: a) rivulet breakup, and b) rivulet profile.

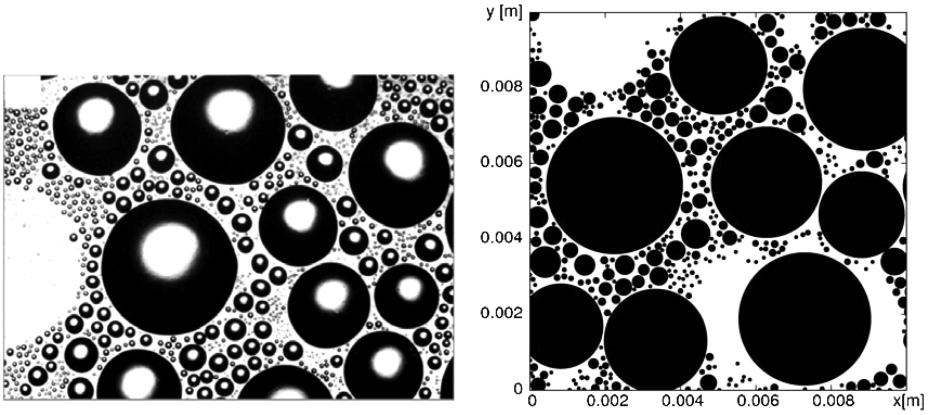

Fig. 6 Typical bead distributions: a) experimental [12], and b) computed.

turn will coalesce and form a film. To investigate the stability of rivulets and film we can refer to the work of Hartley and Murgatroyd [15], who studied theoretically the conditions under which a thin liquid film tends to completely wet a solid surface.

Considering a liquid film flowing on a vertical plate under the effect of gravity and shear stress, we observe that dry patches will form and spread if the mass flow is reduced; consequently, the water begins to flow as rivulets. The process is illustrated in Fig. 5, in which water is flowing from the upper part of the domain and breaks into two rivulets at point B. At point B, if the dry patch is stable, the surface tension must balance the fluid pressure given by the conversion of the kinetic energy of the film upstream (at point A) into static pressure.

Considering AB as a stream tube of transverse width dx, we notice that all the kinetic energy of the water at point A will be converted into a pressure force at point B:

$$\Delta p = \tfrac{1}{2}\rho v^2(x, y) \tag{7}$$

The force exerted by the static pressure of the film along $B_s B_h$ will be the integral of the pressure on the $B_s B_h \mathrm{d}x$ surface, whereas the surface tension opposes it.

Thus, equating surface tension to the pressure force acting on point B and solving for film height, one can find the minimum water-layer height for a continuous film that can exist without disrupting the flow and breaking up into rivulets.

With the same approach we can find the minimum height for a rivulet to flow without separating into smaller beads at the tail when its flow rate is not large enough to sustain the motion of all the water mass belonging to the initial rivulet. Assuming that the rivulet has a cylindrical shape, with a hemispherical head and tail, at the tail the surface tension along the contact line tends to hold and slow the motion of the rivulet, whereas the kinetic energy of the liquid in the core of the rivulet itself promotes the movement of the water.

The force balance is then very similar to the one written to predict film stability; the rigidity force is taken as half of the rigidity of the static bead:

$$F_v = \frac{1}{2}\rho \cdot \iint_{A_{\mathrm{riv}}} \|\bar{v}\|^2 \,\mathrm{d}x\,\mathrm{d}y = f(\sigma, \vartheta, \vartheta_{\mathrm{rec}}, \vartheta_{\mathrm{adv}}, h_{\mathrm{riv}}) = F_\sigma \tag{8}$$

With the aforementioned assumptions on the shape of the rivulet, the integral on the left-hand side can be computed as a function of the local wall shear stress. The complete expression of the function f on the right-hand side is derived from the description of the bead in El Sherbini and Jacobi [13]. Thus, Eq. (8) becomes an algebraic, nonlinear equation in the unknown rivulet height, h_{riv}, that is easily solved via Newton iterations. This allows for the estimate of the minimum rivulet height that, together with the minimum film thickness, can be used as the threshold value to determine the pattern of the water flowing over the iced surface.

We can assume that the beads will first flow either as rivulets or moving beads under the effect of external forces (if the height of the rivulet exceeds the minimum rivulet height), but if the surface water content is large enough to coat the entire surface, a film will form. Moreover, the film can break up into several rivulets if its height is not consistent with the film stability. Depending on the water pattern, we will again modify the evaporation term in the energy equation with the ratio between the actual surface exposed to evaporation and the underlying solid surface.

IV. Results and Discussion

An initial qualitative validation of the Lagrangian model is shown in Fig. 6, in which the computed bead patterns are shown alongside a typical snapshot from Beysens' experiments [12]. The main feature

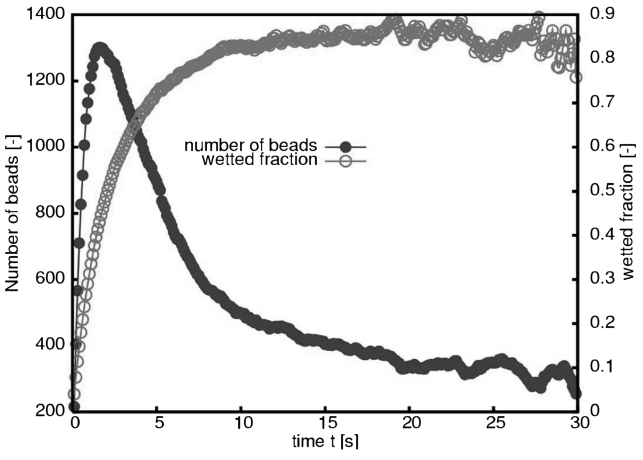

Fig. 7 Wetted fraction vs elapsed time.

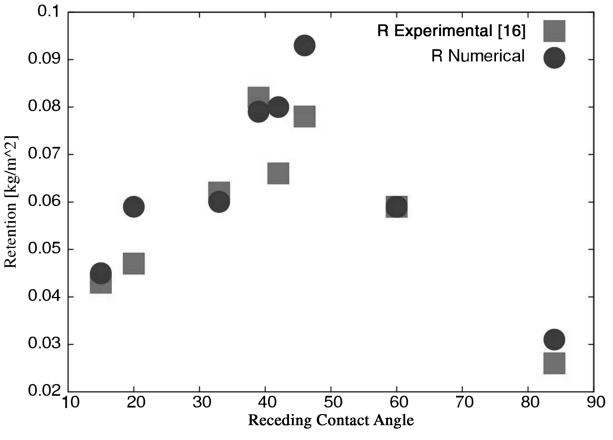

Fig. 8 Warm air validation: water retention on vertical fins.

Table 1 Experimental conditions [1]

Case	T	Velocity	MVD	LWC
5 June 1996	−4.2°C	66.7 m/s	29.8 μm	0.60 g/m^3
30 May 1996	−4.0°C	66.9 m/s	30.2 μm	0.60 g/m^3
10 June 1996	−6.8°C	66.1 m/s	29.8 μm	0.61 g/m^3

of the coalescence, including fractal-like bead distribution, the presence of both wet and dry regions, and the existence of an asymptotic constant value for water coverage (Fig. 7), are correctly captured.

As is becoming the norm rather than the exception in icing multidisciplinary studies, quantitative assessments, such as the accuracy of the coalescence prediction in this case, are given by another discipline, namely, condensation over vertical fins, presented by Min and Webb [16]. No freezing occurs, but we can evaluate the accuracy of both the coalescence model and the motion regime and its threshold, because the experimental evidence shows the presence of a mix of stationary and moving beads. Average quantities such as surface coverage attain a limit cycle, with oscillations around an average value due to the cyclic process of flow and regrowth of some of the beads. A comparison with water retention, that is, the total amount of water trapped on the surface in the form of stationary beads, is shown in Fig. 8. The agreement, for different surface conditions, is quite satisfactory.

A thorough validation of the full roughness model, including CFD code coupling and ice accretion, is more difficult to perform due to the lack of suitable quantitative experimental measurements on beading. However, useful data are provided by Anderson et al. [1], who presented the measurement of the roughness of ice formed during icing tests in the Icing Research Tunnel at the NASA John H. Glenn Research Center at Lewis Field. A NACA 0012 airfoil with 53.3 cm chord was tested at glaze ice conditions; their three experiments are summarized in Table 1. All the tests were conducted at a 0 deg angle of incidence.

The roughness elements were measured from photographs; the roughness element edges had to be inferred from the bright and dark patterns in the images. Because of subjective judgment in defining the size of the elements, many of the images were analyzed by two researchers working independently; thus, the subjective error in defining the roughness element edges, added to the calibration scale error, yields a ±20% maximum error in the reported diameters [1]. The roughness height predicted by the code and that measured in the experiments were compared, assuming that the roughness element height is half of the bead diameter. Because the roughness is evaluated at each time step, in each element, of the ICE3D grid, the roughness variation along the airfoil surface can be plotted as a function of time, as shown in Fig. 9.

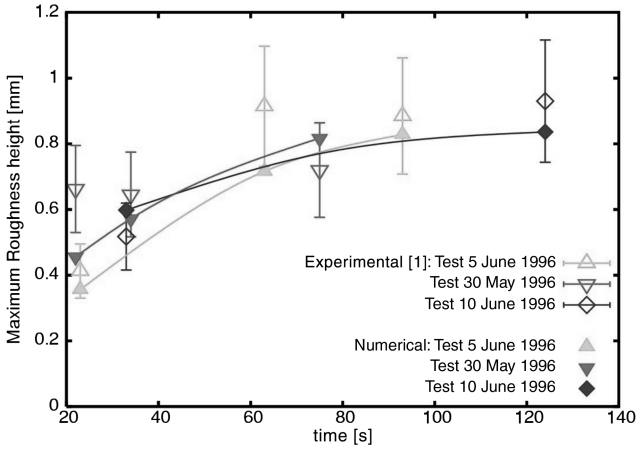

Fig. 10 Maximum roughness height.

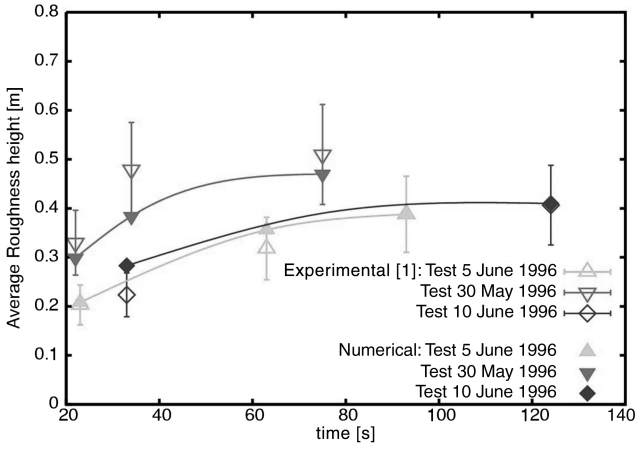

Fig. 11 Average roughness height.

The quantitative results shown in Figs. 10 and 11 are quite encouraging: the computed maximum and average values of roughness are generally well within the experimental uncertainty for all the tests performed and the predicted roughness at the final limit cycle is in very good agreement with experimental data, whereas slight deviations from the experimental values are observed at the onset of ice accretion.

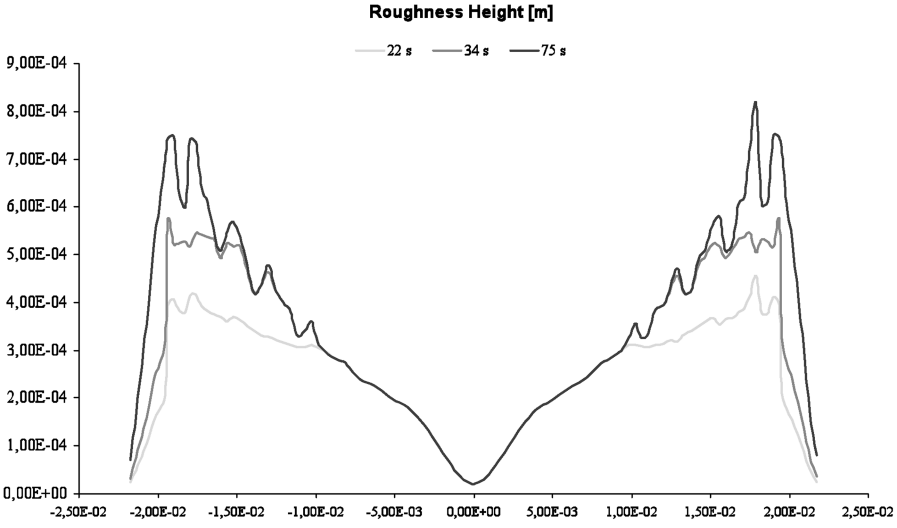

Fig. 9 Ice roughness evolution in space and time.

V. Conclusions

An analysis of the coalescence and dynamic equilibrium of supercooled water droplets at the onset of in-flight ice accretion offers a useful understanding of the physics of the roughness buildup process. In particular, a Lagrangian model that tracks the dynamics of individual beads to simulate the coalescence/motion of beads in a simple geometry was developed to predict the average parameters required by CFD ice growth models, including bead motion threshold and asymptotic water surface coverage. These parameters affect boundary-layer development and heat and mass transfer in active areas of ice accretion.

The use of such quantitative and phenomenological data enables the numerical prediction of the time and space evolution of roughness under icing conditions. A comparison with experimental data shows agreement for both maximum and average roughness values, during bead growth and the final limit cycle, suggesting that the computed distribution is reliable and that the approach is quite promising for use in unsteady ice accretion simulations such as with FENSAP-ICE Unsteady [17].

Further developments are being implemented but not yet tested, including validation of additional transition states (moving beads vs rivulets, rivulets vs film) and the analysis of the impact of space- and time-variable roughness size on the turbulence models and on ice shape predictions. A further investigation of the interaction between growing roughness and the impinging droplets should improve the description of the temporal evolution of the smooth area around the leading-edge stagnation line.

References

[1] Anderson, D. N., Hentschel, D. B., and Ruff, G. A., "Measurement and Correlation of Ice Accretion Roughness," AIAA Paper 98-048, 1998.

[2] Anderson, D. N., and Shin, J., "Characterization of Ice Roughness from Simulated Ice Encounters," AIAA Paper 97-0052, 1997.

[3] Shin, J., "Characteristics of Surface Roughness Associated with Leading Edge Ice Accretion," AIAA Paper 94-0799, 1994.

[4] Bragg, M. B., Kerho, M., and Winkler, J., "Effects of Initial Ice Roughness on Airfoil Aerodynamics," AIAA Paper 94-0800, 1994.

[5] Croce, G., D'Agaro, P., and Della Mora, F., "Numerical Simulation of Glass Fogging and Defogging," *International Journal of Computational Fluid Dynamics*, Vol. 19, 2005, pp. 437–445. doi:10.1080/10618560500233479

[6] Croce, G., De Candido, E., and D'Agaro, P., "Numerical Modeling of Heat and Mass Transfer in Finned Dehumidifiers," *Applied Thermal Engineering*, Vol. 29, 2009, pp. 1366–1374. doi:10.1016/j.applthermaleng.2008.05.003

[7] Shin, J., and Bond, T., "Experimental and Computational Ice Shapes and Resulting Drag Increase for a NACA 0012 Airfoil," NASA Technical Manual 105743, 1992.

[8] Fortin, G., Laforte, J. L., and Illinca, A., "Heat and Mass Transfer During Ice Accretion on Aircrafts Wing with an Improved Roughness Model," *International Journal of Thermal Sciences*, Vol. 45, 2006, pp. 595–606. doi:10.1016/j.ijthermalsci.2005.07.006

[9] Hansman, R. J., and Turnock, S. R., "Investigation of Surface Water Behavior During Glaze Ice Accretion," *Journal of Aircraft*, Vol. 26, No. 2, 1989, pp. 140–147. doi:10.2514/3.45735

[10] Beaugendre, H., Morency, F., and Habashi, W. G., "Development of a Second Generation In-Flight Icing Simulation Code," *Journal of Fluids Engineering*, Vol. 128, No. 2, 2006, pp. 378–387. doi:10.1115/1.2169807

[11] Messinger, B. L., "Equilibrium Temperature of an Unheated Icing Surface as a Function of Airspeed," *Journal of the Aeronautical Sciences*, Vol. 20, No. 1, 1953, pp 29–42.

[12] Beysens, D., "The Formation of Dew," *Atmospheric Research*, Vol. 39, 1995, pp. 215–237. doi:10.1016/0169-8095(95)00015-J

[13] El Sherbini, A. I., and Jacobi, A. M., "Retention Forces and Contact Angles for Critical Liquid Drops on Non-Horizontal Surfaces," *Journal of Colloid and Interface Science*, Vol. 299, 2006, pp. 841–849. doi:10.1016/j.jcis.2006.02.018

[14] Olsen, W., and Walker, E., "Experimental Evidence for Modifying the Current Physical Model for Icing Accretion on Aircraft Structures," NASA TM 87184, 1987.

[15] Hartley, D. E., and Murgatroyd, W., "Critical for the Break-Up of Thin Liquid Layers Flowing Isothermally over Solid Surfaces," *International Journal of Heat and Mass Transfer*, Vol. 7, 1964, pp. 1003–1015. doi:10.1016/0017-9310(64)90042-0

[16] Min, J., and Webb, R. L., "Condensate Formation and Drainage on Typical Fin Materials," *Experimental Thermal and Fluid Science*, Vol. 25, 2001, pp. 101–111. doi:10.1016/S0894-1777(01)00062-0

[17] Aliaga, C. N., Habashi, W. G., Aubé, M. S., Baruzzi, G. S., and Nadarajah, S., "A Third-Generation In-Flight Icing Code: FENSAP-ICE-Unsteady," *SAE Transactions, Journal of Aerospace*, Vol. 116, 2008, pp. 697–703.